Journal of Nuclear Materials 420 (2012) 252–257

Contents lists available at SciVerse ScienceDirect

Journal of Nuclear Materials

journal homepage: www.elsevier.com/locate/jnucmat

Beryllium erosion induced by transient heat loads and subsequent reactions in a deuterium plasma

Shin Kajita [a,*], Daisuke Nishijima [b], Russ Doerner [b], Karl Umstadter [b], Jonathan Yu [b], Noriyasu Ohno [c], Yoshio Ueda [d]

[a] EcoTopia Science Institute, Nagoya University, Nagoya 464-8603, Japan
[b] Center for Energy Research, University of California at San Diego, 9500 Gilman Dr. La Jolla, CA 92093-0417, USA
[c] Graduate School of Engineering, Nagoya University, Nagoya 464-8603, Japan
[d] Graduate School of Engineering, Osaka University, Osaka 565-0871, Japan

ARTICLE INFO

Article history:
Received 18 February 2011
Accepted 28 September 2011
Available online 15 October 2011

ABSTRACT

Pulsed laser irradiation (~0.1–4 MJ/m^2 at 1–10 ms) to a beryllium (Be) target has been performed under steady-state deuterium (D) plasma exposure in the linear divertor plasma simulator PISCES-B to investigate the response of Be to transient heat loads such as edge localized modes. Emission intensities from Be atoms and beryllium deuteride (BeD) molecules are observed in front of the Be target by using two fast framing cameras simultaneously; those exhibit similar time evolution to each other, but spatial profiles are different. While the Be I light emission peaks just in front of the target, the BeD emission peaks away from the target. This indicates that Be atoms are directly ejected from the surface, and BeD molecules are volumetrically formed in the plasma. It is also found that the time evolution of light emission can be qualitatively well reproduced by the evaporation flux of Be atoms, estimated from the calculated surface temperature. The Be surface is thought to be eroded as atoms due mainly to evaporation during laser irradiation.

1. Introduction

Beryllium (Be) will be used as armor tiles of the first wall in ITER, because low-*Z* materials are favorable from the viewpoint of core plasma performance. In addition to steady-state plasma bombardment, Be surfaces will be subjected to transient heat loads accompanied by edge localized modes (ELMs) and disruptions, which may lead to serious damage of the Be first wall. While fundamental researches on steady-state ion or plasma interactions with Be surfaces have been performed using ion beams [1] and linear plasma devices [2,4,3,5], the response of Be surfaces under transient heat loads have hardly been studied.

For tungsten (W) and carbon (C) materials used in the ITER divertor, the effects of transients have been extensively examined using plasma guns [6–9] and pulsed lasers [10–13]. Surface damages such as cracking, melting or sublimation, and arcing have been observed in both plasma gun and pulsed laser experiments. Although laser irradiation does not involve particle bombardment, a temperature excursion induced by ELMs can be simulated by irradiation. It is also worth noting that simultaneous bombardment of laser pulses with steady-state plasma is easily achieved compared to attachment of a plasma gun to a steady-state plasma device.

In this paper, effects of transient heat loads on erosion of a Be target are experimentally investigated in the linear divertor plasma simulator PISCES-B using a pulsed laser irradiation to mimic ELMs. Light emissions from Be atoms and beryllium deuteride (BeD) molecules are simultaneously observed in front of the target during the laser irradiation with two fast framing cameras. Moreover, the temporal evolution of the surface temperature of the Be target is calculated by numerically solving the heat conduction equation, and the evaporation flux of Be atoms is estimated. From comparison between the observations and the calculations, we discuss the dominant erosion process of the Be target during the transients.

2. Setup

2.1. Experimental setup

Fig. 1 shows a schematic of the experimental setup in PISCES-B. Laser pulses from a Nd:YAG laser (NEC: M801C) irradiate a Be target, while the target is exposed to a steady-state deuterium plasma. The incident angle of the laser pulse to the target is 15° with respect to the surface normal, as shown in Fig. 1. The laser wavelength is 1.064 μm, and the temporal evolution of the laser

* Corresponding author.
E-mail address: kajita.shin@nagoya-u.jp (S. Kajita).

0022-3115/$ - see front matter © 2011 Elsevier B.V. All rights reserved.
doi:10.1016/j.jnucmat.2011.09.033

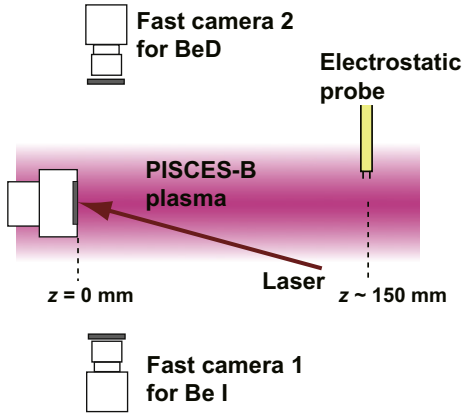

Fig. 1. Schematic of the experimental setup in PISCES-B. The pulsed laser irradiates the Be target, while the target is exposed to the steady-state deuterium plasma. Two fast framing cameras simultaneously observe light emission of Be atoms and BeD molecules with optical filters.

pulse is nominally a rectangular shape. Three different pulse widths, Δt = 1, 3, and 10 ms, were used for investigating the dependence on the pulse width. The energy density of the laser pulse at the target was estimated by considering energy losses due to the transmission of optics and the laser diameter (~2 mm) at the target. The optical reflectivity at the laser wavelength is approximately 55% for an ideal surface [14]. Since the surface was not polished before the experiments, the reflectivity was expected to be lower than 55%. Thus, the absorbed rate was assumed to be 60% to estimate the surface absorbed energy in the present study. The electron density and temperature of the deuterium plasma were measured with an electrostatic double probe at axial position $z \sim 150$ mm away from the target, and were 2.2×10^{18} m^{-3} and 11 ± 3 eV, respectively. The steady-state sample temperature measured by a thermocouple attached to the back side of the sample was ~843 K. The neutral pressure in the vacuum chamber was 6 mTorr. The incident ion energy was set to be ~80 eV by negatively biasing the target with respect to the ground potential.

Two fast framing charge coupled devices (CCDs) were used to observe light emission of Be species in the plasma in response to laser pulses. One is an image intensified CCD camera FASTCAM-MAX I.I. (Photron Co.) and another is a Phantom v7.3 (Vision Research). The two cameras observed emission from the opposite sides of the chamber, as shown in Fig. 1. In front of the cameras, optical filters were placed to detect light emission of the Be I line at 457.3 nm (2^1P-3^1D) and the $A^2\Pi$–$X^2\Sigma^+$ band of BeD (the $\Delta v = 0$ sequence). The central wavelength and FWHM (full width at half maximum) of the optical filter for the Be I line are 457.9 nm and 3 nm, respectively, while those for BeD are 498.7 nm and 3 nm, respectively. The assignment of the molecular band was conducted in a previous study [3] by observing the emission with a spectrometer. Fig. 2 shows typical emission profiles of BeD and Be I. The emission profile of BeD is significantly broader than that of Be I in both axial and vertical directions; the detailed analyses will be given in Section 3.3.

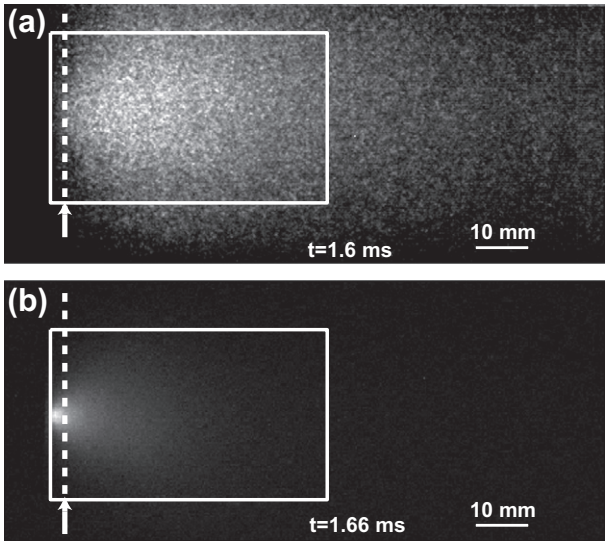

Fig. 2. Typical emission profiles of (a) the A–X band of BeD and (b) Be I at 457.3 nm. Rectangles show the area used for obtaining averaged intensities. Vertical profiles at z = 2 mm, denoted with dotted lines, are plotted in Fig. 7.

2.2. Numerical assessment

The temporal evolution of the material temperature in response to a laser pulse can be calculated from the following heat conduction equation:

$$c_p(T)\rho\frac{\partial T}{\partial t} = \frac{\partial}{\partial z_{mat}}\left(K(T)\frac{\partial T}{\partial z_{mat}}\right) + Q(z_{mat}, t), \quad (1)$$

where c_p is the specific heat in J kg^{-1} K^{-1}; ρ, the mass density in kg m^{-3}; T, the temperature in K; z_{mat}, the distance from the surface in m; and K, the thermal conductivity in W m^{-1} K^{-1}. In Eq. (1), $Q(z_{mat}, t)$ is the power absorbed by metal in W m^{-3}, which is obtained by considering the skin depth in the same manner as in Ref. [10]. The one dimensional heat conduction equation can be applied in this study, because the laser diameter of a few mm is sufficiently greater than the heat conduction length during the laser pulse.

Fig. 3 shows the temperature dependence of K [15], ρ [16], and c_p [17], which are necessary for the calculation. They were extrapolated to the melting point, and the values at the melting point were used at higher temperatures than the melting point. Although it is known that the optical reflectivity slightly decreases with temperature, the effect was neglected in this calculation, because it is minor compared with ambiguities in the reflectivity itself. The thickness of the sample is 1.5 mm, and the temperature gradient at the backside of the sample was assumed to be zero in the calculation.

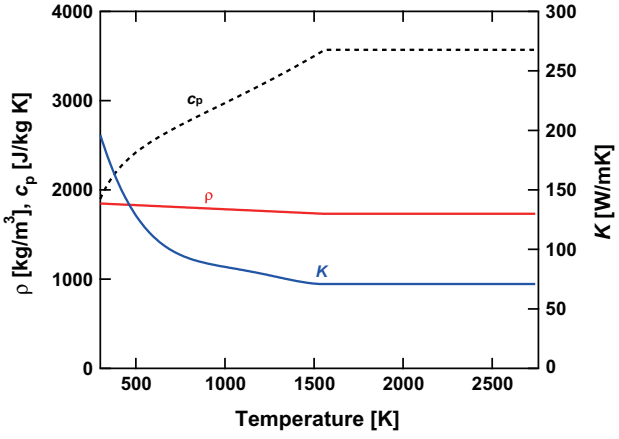

Fig. 3. Temperature dependence of the thermal conductivity, K, specific heat, c_p, and mass density of beryllium, ρ, used in the calculation.

3. Results

3.1. Temporal evolution

Fig. 4a represents the typical temporal evolution of emission intensities of Be I and BeD. The intensities were averaged over the areas shown in Fig. 2. The pulse width and absorbed energy density were 3 ms and ~1.4 MJ m^{-2}, respectively. The laser irradiation starts from 0 ms. The signal intensity gradually increases with time, and the slope changes at $t \sim 1$ ms, where the calculated surface temperature, T_s^{calc}, reaches the melting point, as shown in Fig. 4b. The dips in emission intensities seen at $t \sim 2.7$ ms are probably due to fluctuations of the laser intensity. Shown in Fig. 4c is the flux of evaporating Be atoms given as [18],

$$J_{evap} = \frac{P_v^{calc}}{\sqrt{2\pi M k_B T_s^{calc}}}, \quad (2)$$

where P_v^{calc} is the vapor pressure at T_s^{calc}, M is the atomic mass of Be, and k_B is the Boltzmann constant. The vapor pressure in Ref. [19] was interpolated and used for this estimation. The time evolution of J_{evap} is found to be similar to those of the measured emission intensities. Note that the enhanced erosion of Be due to adatom sublimation [20,21] is not included in the calculation. This process is dominant at surface temperature of ~1100–1450 K, corresponding to $t < 1$ ms in Fig. 4.

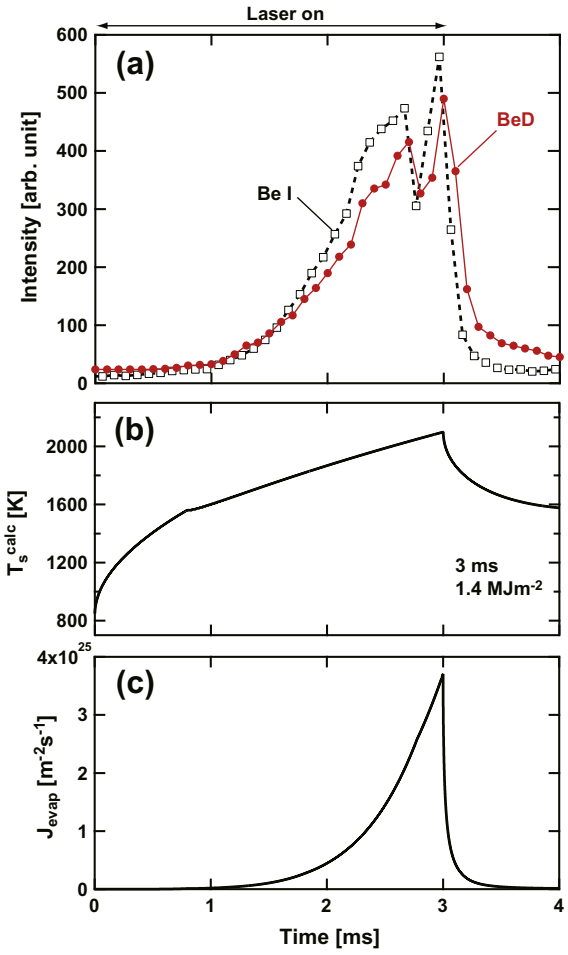

Fig. 4. (a) Temporal evolution of averaged emission intensities of Be I and BeD in response to a laser pulse of 3 ms at 1.4 MJ m^{-2}. The averaged intensities were obtained in the areas shown in Fig. 2a and b. (b) Calculated surface temperature, T_s^{calc}. (c) Calculated evaporation flux of Be atoms from the surface.

3.2. Energy dependence

Fig. 5 shows the surface absorbed energy density dependence of the emission intensities obtained by integrating over the entire emission duration at $\Delta t = 1$ ms, 3 ms, and 10 ms. For both Be I and BeD, comparing the intensities at the same pulse energy, those become smaller, as Δt becomes longer. This is because the power density decreases with an increase in Δt at the same energy. The calculated maximum temperature is plotted as a function of the surface absorbed energy density in Fig. 6a. For instance, at $\Delta t = 3$ ms, the maximum temperature reaches the melting and boiling points at ~0.7 MJ m^{-2} and ~2 MJ m^{-2}, respectively. In Fig. 6b, J_{evap} at the calculated maximum temperature is plotted. Note that the measured Be I intensity at $\Delta t = 3$ ms is ~400 times higher for 1.6 MJ m^{-2} than that for 0.66 MJ m^{-2}, and this factor is nearly consistent with that of J_{evap}.

In this study, because an absolute intensity calibration of the CCD cameras was not conducted, the magnitude of Be I and BeD emission intensities cannot be directly compared. However, the time evolution of relative intensities is enough to discuss the erosion mechanism and subsequent reactions in the plasma for the time being. Further detailed studies will require appropriate theoretical photon emission coefficients of BeD, which are not available at present.

3.3. Spatial profiles

Vertical and axial profiles are obtained from the CCD images used for the analysis in Fig. 4a. The laser pulse width and surface absorbed energy density are 3 ms and 1.4 MJ m^{-2}, respectively.

Fig. 7 shows the vertical emission intensity profiles at various times for (a) BeD and (b) Be I at a distance from the target $z = 2$ mm. It is clearly seen that the vertical profile of BeD is much broader than that of Be I. The temporal evolution of the 1/e widths

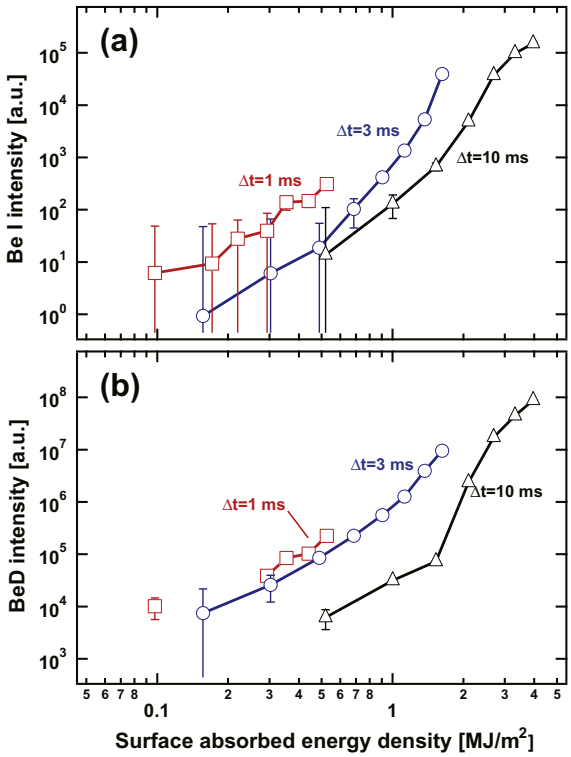

Fig. 5. Surface absorbed energy density dependence of emission intensities of (a) Be I and (b) BeD. The intensities were obtained by integrating over the entire emission duration.

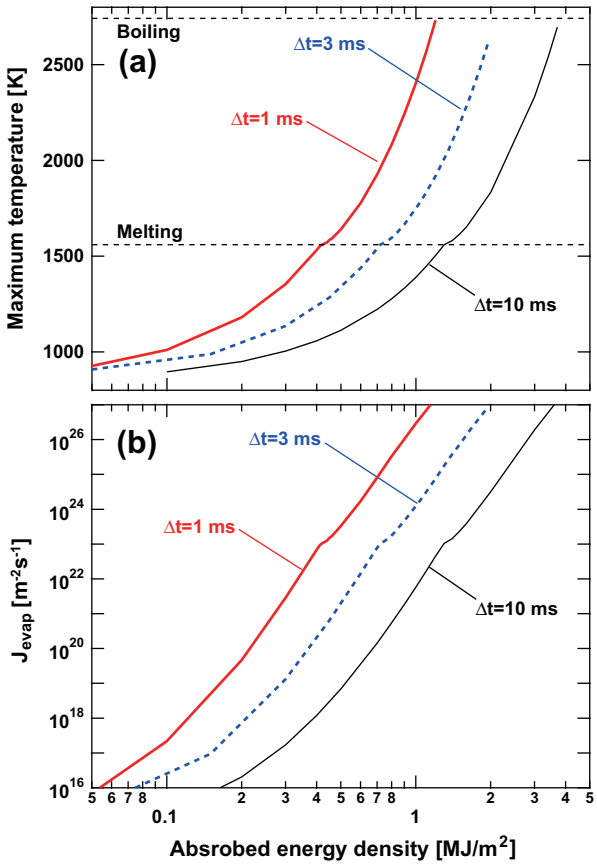

Fig. 6. (a) Calculated maximum temperature as a function of the surface absorbed energy at Δt = 1, 3, and 10 ms. (b) The flux of evaporating Be atoms at the calculated maximum temperature.

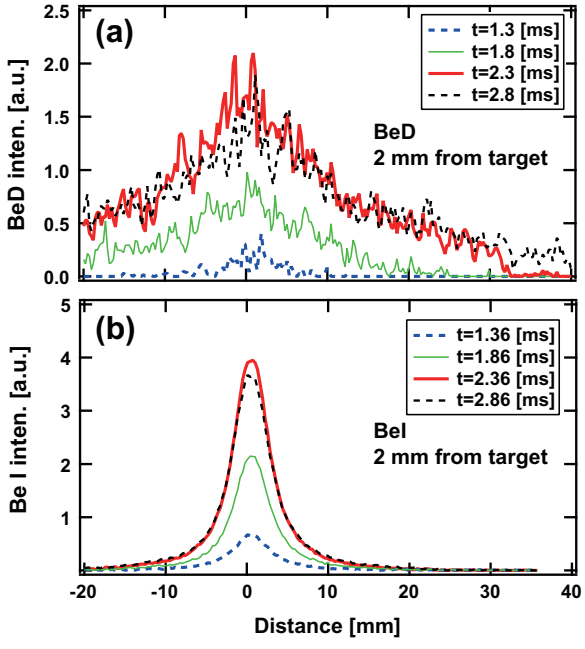

Fig. 7. Vertical intensity profiles of (a) BeD and (b) Be I at various times at z = 2 mm.

of the BeD and Be I vertical profiles at z = 2 mm is shown in Fig. 8. The width of the Be I vertical profile is approximately 4 mm, and does not change during the laser irradiation. On the other hand,

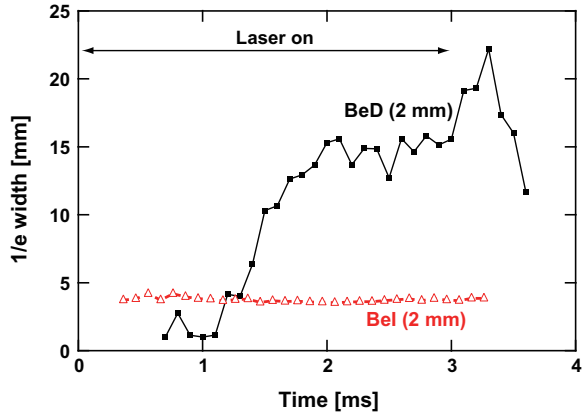

Fig. 8. Temporal evolution of the 1/e width of the vertical emission profiles of BeD and Be I at z = 2 mm.

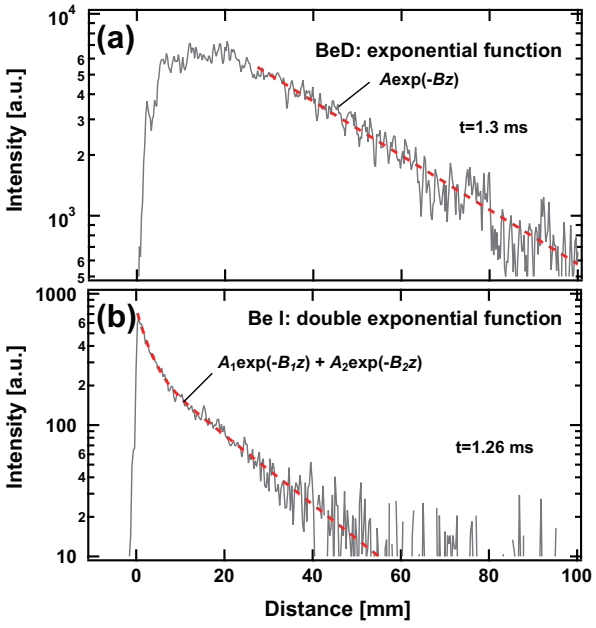

Fig. 9. Axial emission profiles of (a) BeD at t = 1.30 ms and (b) Be I at t = 1.26 ms. Dotted lines in (a) and (b) represent the fitted result using exponential and double exponential functions, respectively.

the width of the BeD profile increases with time from 1 to 2 ms, and becomes constant after 2 ms. This temporal behavior seems to coincide with that of the emission intensity shown in Fig. 4a; the BeD profile becomes broadened, as the intensity increases.

In Fig. 9, axial profiles of BeD and Be I emission intensities at $t \sim 1.3$ ms are plotted. The profiles are taken through the laser irradiation center, and z = 0 mm corresponds to the target position. It should be noted that the Be I profile has a peak just in front of the target, while the BeD intensity gradually increases from z = 0 mm and has a peak at $z \sim 15$–20 mm. Similar to the vertical profiles, the axial profile of BeD is significantly broader than that of Be I. In the region where the BeD intensity decays away from the target, the BeD profile can be well fitted with an exponential function, as shown with a dotted line in Fig. 9a. The Be I profile has two different slopes, and can be fitted with a double exponential function, as demonstrated in Fig. 9b. Fig. 10 shows the time evolution of the 1/e lengths of the BeD and Be I profiles. Similar to the vertical profiles, the 1/e lengths of the Be I axial profile are found to be almost constant during the laser irradiation. On the

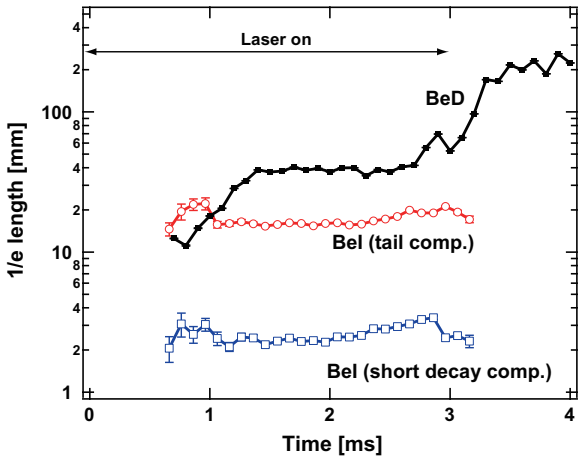

Fig. 10. Temporal evolution of the $1/e$ length of the axial profiles of Be I and BeD. The profile of BeD is fitted with a single exponential function, while that of Be I is fitted with a double exponential function having short decay and tail components.

other hand, the $1/e$ length of BeD increases from $t \sim 1.0$ to 1.5 ms, and becomes almost constant after $t \sim 1.5$ ms until the laser turns off. After the laser irradiation ($t > 3$ ms), the profile becomes nearly flat, since there is no strong ejection of Be from the target.

4. Discussion and summary

In this section, we discuss the dominant erosion process of a Be surface subjected to transient heat loads and reactions of the ejected Be species with background D plasmas based on the observations and the calculations presented above.

The temporal evolution of the measured intensities of Be I and BeD is similar to that of J_{evap} estimated from the calculated surface temperature (see Fig. 4). In addition, the surface absorbed energy density dependence of the Be I and BeD emission intensities is roughly consistent with that of J_{evap}, as demonstrated in Figs. 5 and 6. However, as described in Section 3.3, the spatial profiles of the Be I and BeD light emission are significantly different from each other. While the Be I intensity peaks at $z = 0$ mm and decays quickly, the BeD intensity peaks away from the target and decays gradually. This observation indicates that Be atoms are directly ejected from the surface, while BeD molecules are not ejected directly from the target, but produced in the volume of the plasma. Thus, the Be surface is thought to be eroded as atoms due to evaporation with laser pulses in the parameter range studied here ($\sim$0.1–4 MJ m^{-2} at $\Delta t = 1$–10 ms). Note that the contribution of sputtering as Be atoms and BeD molecules to the measured intensities is negligibly small compared to that of evaporation.

The volumetric formation of BeD was observed in the previous experiment [3], where evaporated Be atoms were injected into steady-state D plasma using a Be effusion cell and strong BeD band emission was then seen. The following reaction chain was proposed for the volumetric formation of BeD molecules:

$$\mathrm{Be} + \mathrm{e} \rightarrow \mathrm{Be}^{+} + \mathrm{e} + \mathrm{e}, \tag{3}$$

and then,

$$\mathrm{Be}^{+} + \mathrm{D}_2 \rightarrow \mathrm{BeD} + \mathrm{D}^{+}. \tag{4}$$

It is highly expected that the same reaction chain can occur with evaporated Be atoms from the target. Since the density of D is estimated to be roughly twentieth of the molecular density [22], the contribution of collisions with D to the formation of BeD is thought to be minor. In the similar manner, collisions with D_2^+ and D^+ are thought to be less frequent as well, because the densities are two orders of magnitude lower than that of D_2. Since the lifetime of BeD excited to $A^2\Pi$ is thought from the strong emission to be significantly short, transport of excited BeD can be negligible. In addition, it is expected that ground state BeD is predominantly produced by the process as given by Eq. (4). Thus, electron impact excitation of BeD would dominate the spatial profiles of BeD emission.

In Refs. [3–5], it has been found that Be surfaces are sputtered as BeD molecules as well as Be atoms and that the sputtered flux of BeD molecules peaks at surface temperature of $\sim$440 K. The steady-state surface temperature was $\sim$843 K in this experiment, and the calculation predicts higher temperatures during a laser pulse. Thus, it is reasonable that BeD molecules are not ejected from the surface during the laser irradiation. In addition, it has been reported that the axial profile of the emission intensity of sputtered BeD molecules peaks just in front of the target [3,4], which differs from the observation here.

The difference in the spatial profiles between Be I and BeD emission may be explained by the reaction chain above. The ionization mean free path of evaporated Be atoms, λ_{mfp}, is expressed as,

$$\lambda_{mfp} = \frac{v_{Be}}{\langle \sigma v \rangle_i n_e}, \tag{5}$$

where v_{Be} is the ejected (evaporated) Be atom velocity and $\langle \sigma v \rangle_i$ ($\sim 5 \times 10^{-14}$ m^3/s at $T_e = 11$ eV and $n_e = 2 \times 10^{18}$ m^{-3} [23]) is the ionization rate coefficient of Be. At surface temperature of $\sim$1500–2000 K, $v_{Be} \sim (1.7 - 1.9) \times 10^3$ m/s, and λ_{mfp} is estimated to be $\sim$17–19 mm, which is consistent with the tail component of the Be I axial $1/e$ length (see Fig. 10). The short decay component in front of the target is much shorter than the tail one, and might be due to a high density Be plasma produced during laser irradiation. This hypothesis needs to be confirmed by local measurements of n_e and T_e in front of the target. In addition to the ionization process, the following charge exchange process may occur [24]:

$$\mathrm{Be} + \mathrm{D}^{+} \rightarrow \mathrm{Be}^{+} + \mathrm{D}. \tag{6}$$

This process also contributes to the formation of Be^+.

According to the reaction as expressed by Eq. (4), the spatial profile of BeD emission intensity is predominantly determined by that of Be^+. As mentioned above, the source of Be^+ ions is ionization and charge exchange of Be atoms. This means that the initial profile of Be^+ is spatially extended, while the source of Be atoms is limited to the laser irradiated spot on the Be surface. Moreover, since Be^+ ions are heated up due to Coulomb collisions with the background plasma more efficiently than Be atoms, the temperature and velocity of Be^+ should be higher than those of Be. In addition, the higher ionization potential (18.2 eV) of Be^+ than Be (9.3 eV) can contribute to the further expansion of the spatial profile of Be^+, since the ionization loss of Be^+ ions is less effective. It should be noted that cross-field diffusion of Be^+ is expected to be rather fast because of the large Larmor radius of $\sim$20–40 mm at assumed ion temperature of $\sim$0.2–1.0 eV.

As can be seen in Figs. 8 and 10, the $1/e$ width and length of the Be I emission profiles are nearly constant, while those of BeD change in time. This also supports that BeD molecules are subsequently formed in the plasma due to the reaction chain described above. It is worth noting that the $1/e$ length of BeD reaches the equilibrium faster than the $1/e$ width. This may be attributed to the higher mobility of Be^+ along the magnetic field.

In summary, the response of Be to transient heat loads provided by a pulsed laser has been investigated under steady-state D plasma bombardment in PISCES-B. Evaporation is thought to be the dominant erosion process of Be during the transients ($\sim$0.1–4 MJ m^{-2} at 1–10 ms). Since the surface is heated by the transients, BeD molecules are not directly ejected from the surface, but created in the plasma through the atomic and molecular processes.

Although only a bulk Be target was used in this study, deposited Be layers will be formed on Be as well as on C and W divertor target surfaces, and Be-C [25] and Be-W [26] mixed materials can be created in ITER. Thus, it is of significant importance to explore the interaction of the deposited Be layers and mixed materials with transients.

Acknowledgements

The authors thank PISCES research and technical staff for their dedicated support. This work was conducted under the Japan–US cooperation in Fusion Research and Development.

References

[1] J. Roth, W. Eckstein, M. Guseva, Fus. Eng. Des. 37 (1997) 465.
[2] R.P. Doerner, A. Grossman, S. Luckhardt, R. Seraydarian, F.C. Sze, D.G. Whyte, R.W. Conn, J. Nucl. Mater. 257 (1998) 51.
[3] D. Nishijima, R.P. Doerner, M.J. Baldwin, G.D. Temmerman, E.M. Hollmann, Plasma Phys. Control. Fusion 50 (2008) 125007.
[4] R.P. Doerner, M.J. Baldwin, D. Buchenauer, G.D. Temmerman, D. Nishijima, J. Nucl. Mater. 390–391 (2009) 681.
[5] D. Nishijima, R.P. Doerner, M.J. Baldwin, G.D. Temmerman, J. Nucl. Mater. 390–391 (2009) 132.
[6] V.I. Tereshin, I.E. Garkusha, A.N. Bandura, O.V. Byrka, V.V. Chebotarev, V.A. Makhlaj, D.G. Solyakov, H. Wuerz, J. Nucl. Mater. 313–316 (2003) 685.
[7] I. Garkusha, A. Bandura, O. Byrka, V. Chebotarev, I. Landman, V. Makhlaj, A. Marchenko, D. Solyakov, V. Tereshin, S. Trubchaninov, A. Tsarenko, J. Nucl. Mater. 337–339 (2005) 707.
[8] Y. Kikuchi, D. Nishijima, M. Nakatsuka, K. Ando, T. Higashi, Y. Ueno, M. Ishihara, K. Shoda, M. Nagata, T. Kawai, Y. Ueda, N. Fukumoto, R. Doerner, J. Nucl. Mater. 415 (2011) S55.
[9] D. Nishijima, Y. Kikuchi, M. Nakatsuka, M. Baldwin, R. Doerner, M. Nagata, Y. Ueda, Fusion Sci. Technol. 60 (2011) 1447.
[10] S. Kajita, S. Takamura, N. Ohno, D. Nishijima, H. Iwakiri, N. Yoshida, Nucl. Fusion 47 (2007) 1358.
[11] Y. Ueda, M. Toda, M. Nishikawa, K. Kondo, K. Tanaka, Fus. Eng. Des. 82 (2007) 1904.
[12] S. Kajita, S. Takamura, N. Ohno, Nucl. Fusion 49 (2009) 032002.
[13] K. Umstadter, R. Doerner, G. Tynan, Phys. Scr. T138 (2009) 014047.
[14] Landolt-Börnstein Numerical Data and Functional Relationships in Science and Technology Group III, vol. 15, Springer, 1985.
[15] L. Berg, G. Czack, D. Gras, E. Koch-Bienemann, Gmelin Handbook of Inorganic and Organometallic Chemistry (Beryllium), eighth ed., vol. suppl. A2, Springer, Berlin, 1991.
[16] Japan Society of Thermophysical Properties, Thermophysical Property Handbook, Yokendo, Tokyo, 2000.
[17] The Japan Institute of Metals, Kinzoku Databook second ed., Maruzen, Tokyo, 1984.
[18] A. Anders, Cathodic Arcs: From Fractal Spots to Energetic Condensation, first ed., Springer, 2008.
[19] R.E. Honig, D.A. Kramer, RCA Rev. 30 (1969) 285.
[20] R.P. Doerner, S.I. Krasheninnikov, K. Schmid, J. Appl. Phys. 95 (2004) 4471.
[21] R.P. Doerner, M.J. Baldwin, S.I. Krasheninnikov, K. Schmid, J. Nucl. Mater. 337-339 (2005) 877.
[22] D.G. Whyte, R.P. Seraydarian, R.P. Doerner, J. Vac. Sci. Technol. A 17 (1999) 2713.
[23] H.P. Summers, The Atomic Data and Analysis Structure User Manual, Version 2.6, 2004. <http://www.adas.phys.strath.ac.uk>.
[24] P. Barragan, L.F. Errea, L. Mendez, I. Rabadan, A. Riera, J. Phys. B: At. Mol. Opt. Phys. 41 (2008) 225202.
[25] M.J. Baldwin, R.P. Doerner, Nucl. Fusion 2006 (2006) 444.
[26] M.J. Baldwin, R.P. Doerner, D. Nishijima, D. Buchenauer, W.M. Clift, R.A. Causey, K. Schmid, J. Nucl. Mater. 363–365 (2007) 1179.